Baghdad Science Journal

Volume 22 | Issue 6 Article 17

6-20-2025

Thermal Simulation for Ultrafast Laser in Multilayered Sample for Heat-Assisted Magnetic Recording Application

Haidar J. Mohamad
Department of Physics, College of Science, Mustansiriyah University, Baghdad, Iraq,
haidar.mohamad@uomustansiriyah.edu.iq

Basaad Hadi Hamza
Department of Physics, College of Science, Mustansiriyah University, Baghdad, Iraq,
bassaadhadi@uomustansiriyah.edu.iq

Follow this and additional works at: https://bsj.uobaghdad.edu.iq/home

How to Cite this Article

Mohamad, Haidar J. and Hamza, Basaad Hadi (2025) "Thermal Simulation for Ultrafast Laser in Multilayered Sample for Heat-Assisted Magnetic Recording Application," *Baghdad Science Journal*: Vol. 22: Iss. 6, Article 17.
DOI: https://doi.org/10.21123/2411-7986.4967

This Article is brought to you for free and open access by Baghdad Science Journal. It has been accepted for inclusion in Baghdad Science Journal by an authorized editor of Baghdad Science Journal.

BAGHDAD SCIENCE JOURNAL 2025;22(6):1930–1939

Scan the QR to view
the full-text article on
the journal website

RESEARCH ARTICLE

Thermal Simulation for Ultrafast Laser in Multilayered Sample for Heat-Assisted Magnetic Recording Application

Haidar J. Mohamad *, **Basaad Hadi Hamza**

Department of Physics, College of Science, Mustansiriyah University, Baghdad, Iraq

ABSTRACT

Heat-Assisted Magnetic Recording (HAMR) is a promising step in expanding hard disk capacity. This technique depends on the ultrafast laser to demagnetize the layer and record the data on a hard disk or any storage media. However, the recipe for the layers is challenging and gives a space to explore. The investigation of the effects of temperature profile and thermal gradient on the suggested sample FePt (8 nm)/MgO (8 nm)/SiO_2 (58 nm)/Si (9.32 E-7 m) for HAMR use was the focus of this study. The simulation of the multilayered gives a view of ultrafast laser behavior (power density 1.7923 E14 W/m^2 with an 800 nm wavelength) inside the sample stack. The optical consideration is calculated depending on the incident, reflected, and transmitted light on the surface between layers. Sample layer thickness plays a crucial role in reducing laser power. The temperature gradient inside the sample helps choose the appropriate laser power, which is used with the HAMR technique. Results show the influence of temperature on sample thickness and temperature as laser power. Then, it is obvious which thickness and power laser can be used efficiently.

Keywords: Data storage, HAMR technique, Optical simulation, Spintronic device, Ultrafast laser

Introduction

Heat-Assisted Magnetic Recording (HAMR) technique records a data on a storage medium. This method employs a laser to reduce magnetization on a femtosecond timescale to record the data. Laser power generates heat in the storage sample which reduces the coercive field in an inverse proportional relationship. Therefore, the sample layers must have a high magneto-crystalline anisotropy.

The hysteresis loop has been studied for the FePt layer and configured for the spin direction of this alloy. A small coercivity field is useful to reverse the magnetization direction quickly for this alloy by laser heat. This gives the benefit of recording stable data with a weak magnetic field. Laser power influence time has been investigated with the HAMR technique.[1] Demagnetization happens within a short time during laser power interaction with the sample surface. Demagnetization time is a vital parameter investigated in this work.

Researchers used the FePt sample as a magnetic recording medium because it has high coercivity. The melting temperature is about 1830 K and has high magneto-crystalline anisotropy. Therefore, it has been recommended to sputter SiO_2 as it has a higher thermal stability to be fabricated with the FePt process.[2,3] Different methods were used to fabricate SiO_2 like Sol-Gel,[4] spark plasma sintering,[5] and the green method,[6] and it has been shown that it has high temperatures and high pressures.[7] MgO is used as a thermal interface material for electronic devices to achieve good heat dissipation.[8] MgO sample has a high stable temperature, low heat capacity, thermal

Received 21 May 2024; revised 20 October 2024; accepted 22 October 2024.
Available online 20 June 2025

* Corresponding author.
E-mail addresses: Haidar.mohamad@uomustansiriyah.edu.iq (H. J. Mohamad), bassaadhadi@uomustansiriyah.edu.iq (B. H. Hamza).

https://doi.org/10.21123/2411-7986.4967
2411-7986/© 2025 The Author(s). Published by College of Science for Women, University of Baghdad. This is an open-access article distributed under the terms of the Creative Commons Attribution 4.0 International License, which permits unrestricted use, distribution, and reproduction in any medium, provided the original work is properly cited.

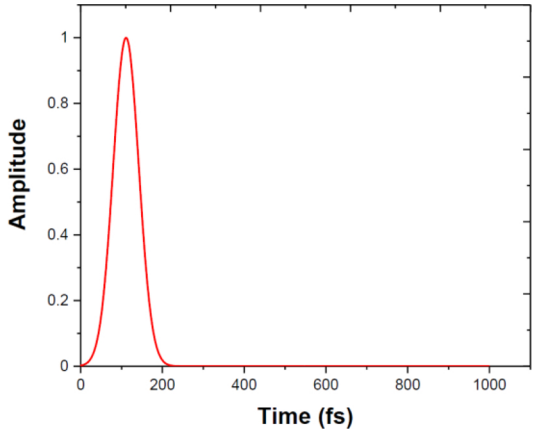

Fig. 1. Gaussian peak power laser shape used in the simulation.

conductivity of about 60 W/mK, and high melting point. It is synthesized using the precipitation method to get nanoparticles.[9]

HAMR technique details have been summarized and discussed, for instance, by H. Sepehri-Amin et al. (2018) which investigated FePt/C, SiO_2/MgTiO (MgO) samples for HAMR use. They measured the microstructure and magnetic properties and compared them between all samples. Heat diffusion was not discussed in their work as was the behavior of the recording media.[10]

A. Meo et al.[11] investigated the FePt grain magnetization dynamics and temperature with applied field using the Landau-Lifshitz-Bloch equation. They simulated an atomic spin model to support their opinion about HAMR dynamics with the suggested sample. They simulated one sample (FePt) with $5 \times 5 \times 10$ nm^2 dimensions to suggest the mechanism of temperature pulse. Muhaiman A. et al.[12] presented a 3-D simulation of the HAMR technique using a FeNi/Cu/YIG/GGG multilayered sample. The spin current is discussed as well as the effect of changing the magnetic layer thickness as a function of a femtosecond laser. Spin diffusion and optical equations are simulated which explain the behavior of the laser inside the sample. Tom et al.[13] investigated the optical forces in HAMR by changing the head-disk spacing for Pt and SiO_2. They examined spacings 8 nm, 4 nm, and 2 nm where the simulations tend to emphasize the importance of the spacing and the magnitude influence of the force. Yifei Chen and R. H. Victora[14] simulated a pulsed laser instead of a continuous laser. They show that the synchronization between laser pulses and magnetic fields tends to enhance thermal gradients in the sample.

The investigation of the effects of temperature profile and thermal gradient on the suggested sample (FePt/MgO/SiO_2/Si) for HAMR use was the focus of this study. The ultrafast pulsed laser of 800 nm was simulated using COMSOL software (v. 6.0), and its penetration through the sample layers was analyzed. The incident, reflecting, and transmitted beams were considered according to the multilayer optical model.

Materials and methods

The simulation of the suggested sample, FePt (8 nm)/MgO (8 nm)/SiO_2 (58 nm)/Si (9.32 E-7 m), was performed using COMSOL software (v.6.0). The simulation consists of two stages. First, a calculation of the incident, reflected and transmitted light through multilayers (MATLAB code was used to support simulation). The light used is an ultrafast pulsed laser with 800 nm wavelength, 120 μm spot laser diameter, FWHM pulse laser width (t) 74 fs, and repetition rate (f) 100 kHz. Therefore, the peak power with the Gaussian pulse beam assumed in the simulation is shown in Fig. 1 using P = power (mW)/(f*t). The power is fixed at 15 mW in the simulation steps.

Second, temperature gradient simulation using the heat diffusion equation.[15] The electric field is distributed in the sample layers, therefore an optical model of transmitted/reflected coefficients at layer interfaces is used. The time scale of the laser is in femtoseconds, therefore a rapid increase in temperature needs to be explained in three dimensions of the heat diffusion equation. The temperature behavior inside

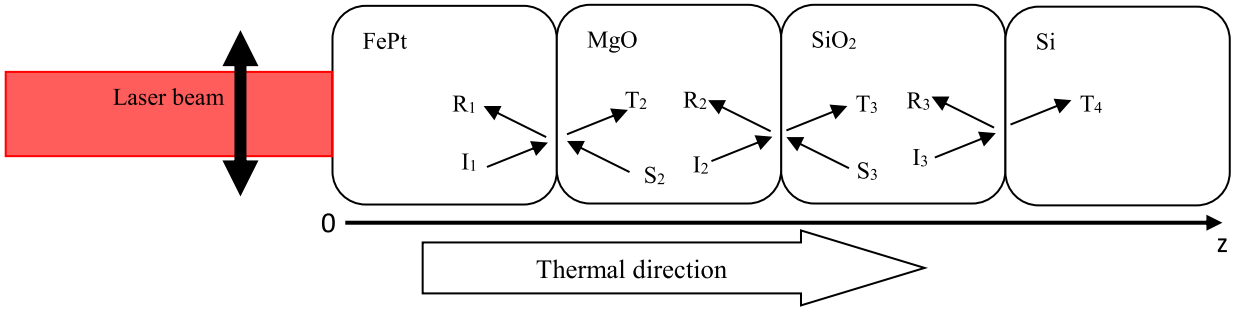

Fig. 2. Reflected/transmitted model used in the simulation, where R, I, T, and S are the reflected, incident, transmitted, and light reflected from the next surface layer, respectively.

the sample can be described as[16]:

$$\frac{1}{D}\frac{\partial T}{\partial t} = \frac{\partial^2 T}{\partial x^2} + \frac{\partial^2 T}{\partial y^2} + \frac{\partial^2 T}{\partial z^2} + \frac{g(x,\ y,\ z,t)}{k} \quad (1)$$

where D represents the thermal diffusivity ($D = (k/\rho)\ C_p$) where k is the thermal conductivity, ρ is the density of the material, C_p is the heat capacity per unit mass, and $g(x,\ y,\ z,t)$ is the absorbed power density within the sample.

The heat source (pulsed laser) in Eq. (1) and the temperature distribution at each layer are determined by an electric field. The propagation of the electric field is modeled with multi-reflected/transmitted at sample interfaces and is shown in Fig. 2.

The simulation depends on the field amplitude at each layer. For the first layer, the field amplitude of incident and reflected light is[17]:

$$R_s = \left[\frac{E_r}{E_i}\right]^2 = \left[\frac{n_1 cos\theta_i - n_2 cos\theta_t}{n_1 cos\theta_i + n_2 cos\theta_t}\right]^2, \quad (2)$$

$$R_p = \left[\frac{E_r}{E_i}\right]^2 = \left[\frac{n_1 cos\theta_t - n_2 cos\theta_i}{n_1 cos\theta_t + n_2 cos\theta_i}\right]^2 \quad (3)$$

They are related to the transmission coefficients through:

$T_s = 1 - R_s$ and $T_p = 1 - R_p$

For the case of normal incident light on a flat surface, the above equations reduce to the more familiar equation $R = R_s = R_p$ then[17]:

$$\mathrm{R} = \left(\frac{n_1 - n_2}{n_1 + n_2}\right)^2, \quad (4)$$

The reflectivity of a given material will depend on the frequency of the light source through the dispersion relation of its index of refraction.

Once inside the material, absorption causes the intensity of the light to decay with depth at a rate determined by the material's absorption coefficient. In general, is a function of wavelength and temperature, but for constant, the intensity I decays exponentially with depth z according to the Beer–Lambert law[17]:

$$I_z = I_0 e^{-\alpha z} \quad (5)$$

where I_0 is the intensity just inside the surface after considering reflection loss. The transmission of light can be expressed as[18]:

$$T_{ij} = \frac{2n_i cos\theta_i}{n_j cos\theta_i + n_i cos\theta_j} \quad (6)$$

The layer matrix L_j also known as phase matrix, describes the propagation of light through the layer j. It is expressed in terms of parameters of j^{th} layer N_j,

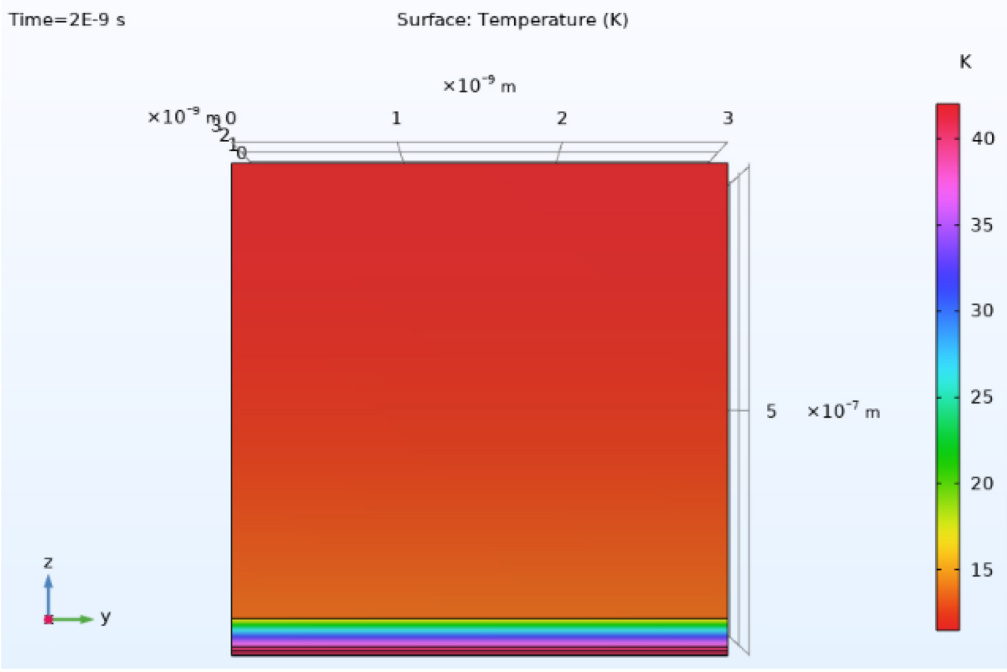

Fig. 3. Temperature distribution inside the suggested sample with different time delays. In this data, the thermal boundary resistance (TBR) is included.

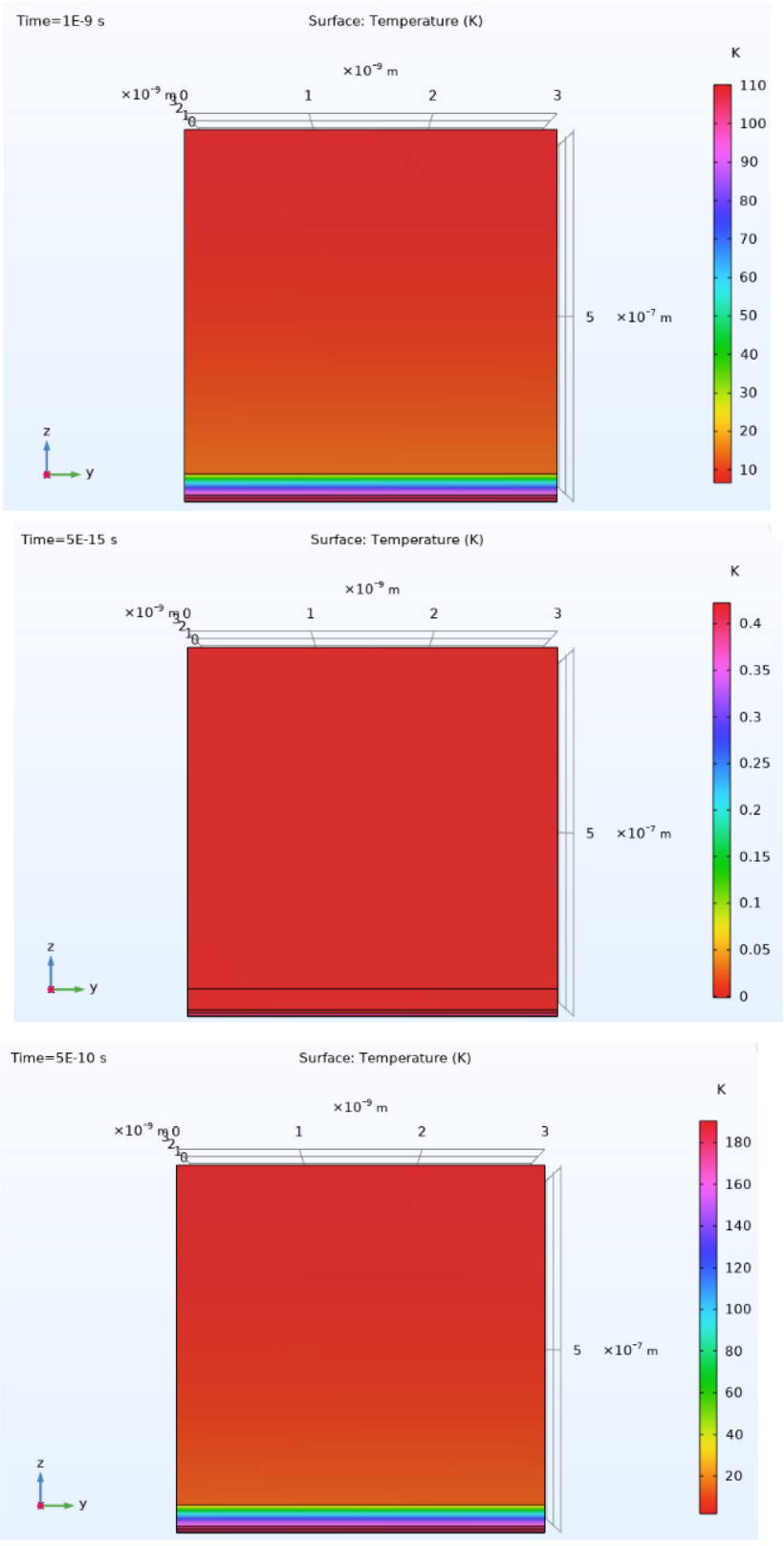

Fig. 3. Continued.

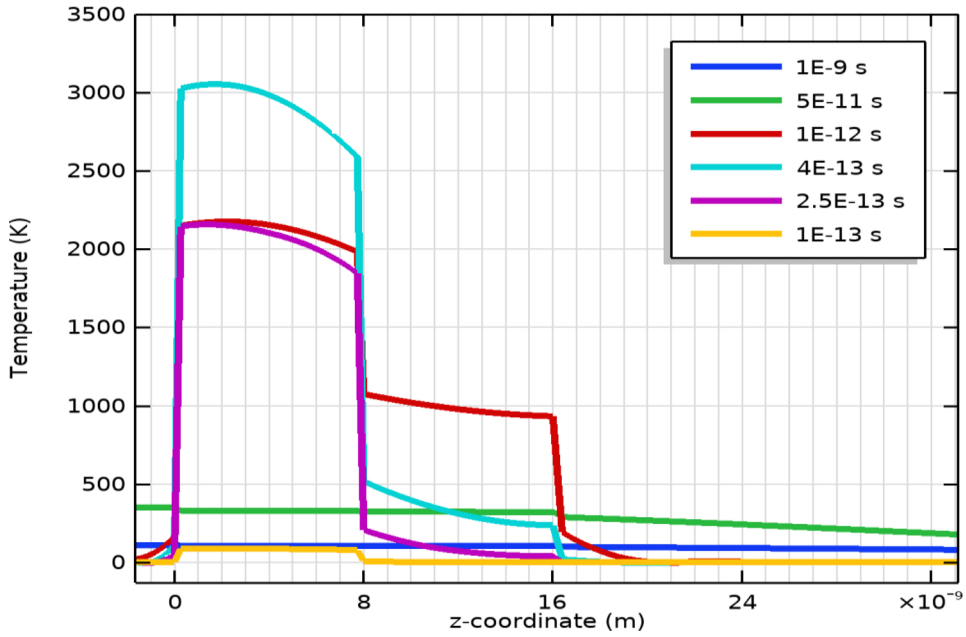

Fig. 4. Temperature with the suggested sample at selected time delays. TBR is considered.

and θ_j as[18]:

$$L_j = \begin{bmatrix} Z_j & 0 \\ 0 & Z_j^{-1} \end{bmatrix} \quad (7)$$

where

$$Z_j = \exp\left(\frac{2\pi i d_j}{\lambda} N_j \cos\theta_j\right) \quad (8)$$

The simulation depends on the field amplitude at each layer. For the first layer, the field amplitude of incident and reflected light is[18]:

$$\boldsymbol{E}_i^1 = I_1 e^{\gamma_1 z} \boldsymbol{X} \quad (9)$$

$$\boldsymbol{E}_r^1 = R_1 e^{-\gamma_1 z} \boldsymbol{X} \quad (10)$$

where $\gamma = j\omega\sqrt{\mu\varepsilon} = j\frac{2\pi}{\lambda}\tilde{n} = jk_0(n + jk)$, $\tilde{n}$ is the complex refractive index, k_0 is the wavenumber, n, and k are the real and imaginary parts of the refractive index, and $\boldsymbol{X}$ is the wave unit vector.

Material properties

The material properties are important to achieve accurate simulation like thermal conductivity, material density, heat capacity, and refractive index with two parts real and imaginary. These data are used in the optical absorption and thermal distribution inside the sample. These properties are listed in Table 1.

Thermal boundary resistance (TBR) interface conditions are considered in the simulation study because the temperature profile changed significantly without considering this value. However, this value describes the interface between two different layers, and it is not well understood because it is varied according to the fabrication process or method.[25] Table 2 consists of the values used in the simulation for the TBR.

Table 2. Thermal boundary resistance values used in the calculations for the suggested sample.

Interface	TBR (m^2K/W)
FePt/ MgO	3.5×10^{-9}
MgO/ SiO_2	3.38×10^{-9}
SiO_2/Si	3.84×10^{-9} [26]

Temperature configuration in 3-D thermal model

The thermal description inside the suggested sample, which is caused by a focused ultrafast

Table 1. Sample layers properties were used in the simulation.

Material	Density (Kg/m^3)	Thermal conductivity (W/(m.K))	Specific Heat capacity (J/Kg.K)	Refractive index
FePt	14900	13[19]	11.2	N = 3.6 + i5
MgO	3580[20]	30[21]	41.71	1.736
SiO2	2650	1.1[22]	68.95	1.47 + i 0.2[23]
Si	2329	150[24]	143	3.56

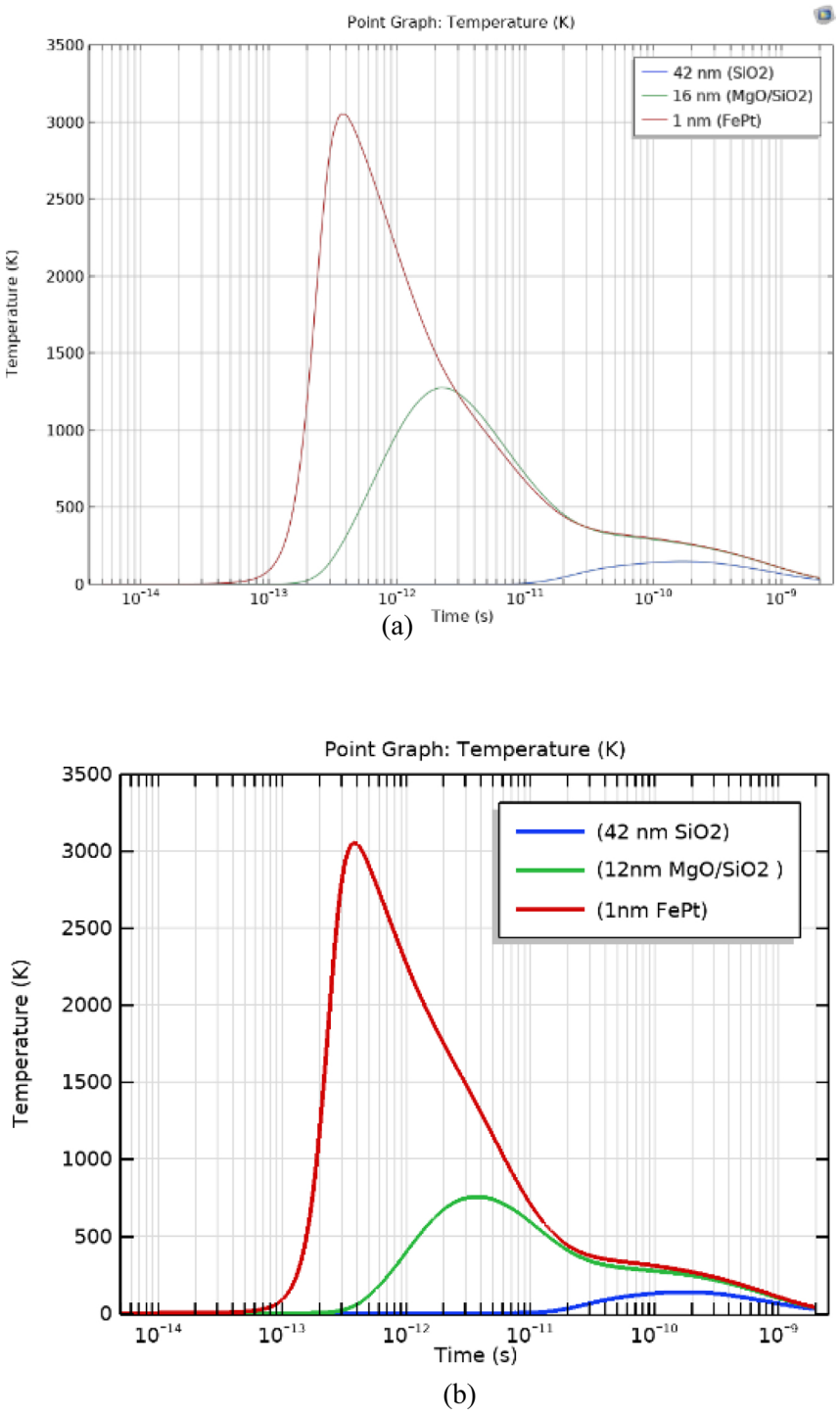

Fig. 5. Temperature behavior with time at some points inside the suggested sample (a) MgO is 8 nm, and (b) MgO is 4 nm thickness. Thermal boundary resistance (TBR) is considered.

laser beam, can be modeled in a 1-D configuration. This configuration is not sufficient to describe the thermal distribution, therefore a 3-D model is used to simulate thermal behavior in this work. The 3-D model allows us to use thermal equations, thermal boundary conditions, and optical equations described earlier and calculate the temperature profile for the suggested sample simultaneously.

In COMSOL software, the thermal equation used to describe the temperature time dependent inside

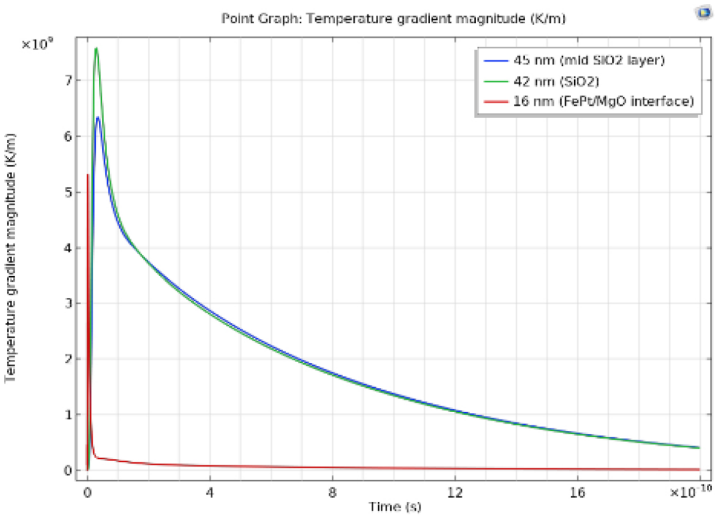

(a)

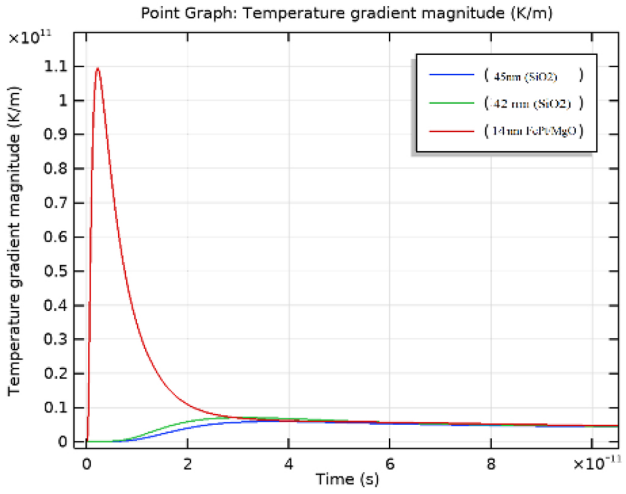

(b)

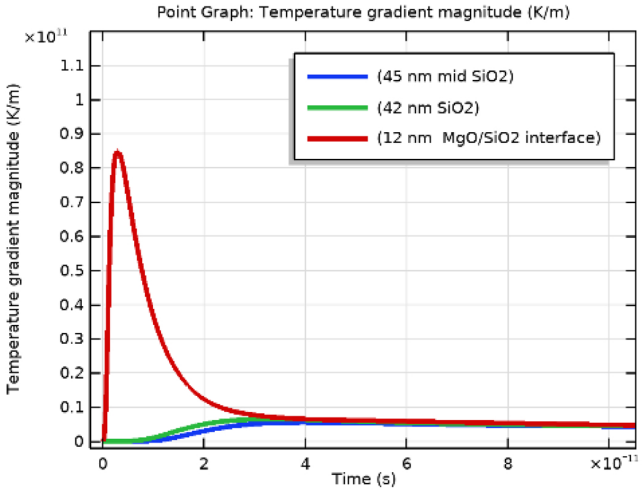

(c)

Fig. 6. Temperature gradient with time inside some points of the suggested sample(a) MgO is 8 nm, (b) MgO is 6 nm, and (c) MgO is 4 nm thickness. Thermal boundary resistance (TBR) is considered.

the sample with 3D configuration can be represented as[16]:

$$\rho C_p \frac{\partial T}{\partial t} = Q + \nabla.\left(k \nabla T\right) \quad (11)$$

where ρ is material density (kg/m^3), C_p is the specific heat capacity (J/(kg·K)), T is the temperature in Kelvin, k is thermal conductivity (W/m. K), Q is laser energy density (W/m^3).

Results and discussion

The simulation calculates laser heating inside the sample depending on material properties. The temperature distribution is related to a femtosecond pulsed laser with a power density of 1.7923 E14 W/m^2 and 800 nm wavelength. Fig. 3 shows the sample's temperature behavior at different delay times.

The temperature change as a function of sample thickness caused by a femtosecond pulsed laser is shown in Fig. 4 with different time intervals. A high rise in the temperature in the FePt layer affects the MgO layer, this generates a thermal gradient in SiO_2 layer at a time of 0.05 and 1 ns. The behavior in temperature within the sample changes if we neglect the thermal boundary resistance (TBR) values, therefore it is important to include TBR values in calculations. There was no significant change in Fig. 4 when MgO thickness was changed. The effect is noticeable at the interface and cannot be clearly noticed within this figure.

Fig. 5 shows the temperature at selected points in the specimen with TBR value. The temperature transfers from FePt to SiO_2 through the MgO layer around 1 ns. The interface between the MgO and SiO_2 has high temperatures in a time scale of 0.05 ns with the help of the thermal boundary resistance (TBR) value. The temperature gradient is changed at the interface of MgO and SiO_2.

Fig. 6 shows the temperature gradient as a function of time at certain points inside the suggested sample. The influence of thermal boundary resistance (TBR) value is vital in the presence of a thermal gradient. The thickness change in MgO plays an important role in changing the temperature at the interface between MgO and SiO_2 as well as at SiO_2 thickness.

Conclusion

A multilayer sample is suggested to be a candidate for HAMR use. A simulation using COMSOL software helps to understand the temperature behavior of the laser pulse. The femtosecond pulsed laser is simulated depending on the reflected, transmitted, and absorbed laser light. The pulsed laser has a significant impact on the temperature rise in the FePt layer. This layer gains the power of the incoming light and transfers it to the next layer MgO. The important time scale is 0.05 and 1 ns because of the fast process like spin current or demagnetization scale time range within this time. The laser power depends on the layer's thickness which gives a high temperature gradient within the sample layers and leads to saving energy.

Acknowledgment

The authors express their gratitude to the Department of Physics at the College of Science, Mustansiriyah University (www.uomustansiriyah.edu.iq) in Baghdad, Iraq, for their support in the current research.

Authors' declaration

- Conflicts of Interest: None.
- We hereby confirm that all the Figures and Tables in the manuscript are ours. Furthermore, any Figures and images, that are not ours, have been included with the necessary permission for republication, which is attached to the manuscript.
- No animal studies are present in the manuscript.
- No human studies are present in the manuscript.
- Ethical Clearance: The project was approved by the local ethical committee at Mustansiriyah University.

Authors' contribution statement

Authors contributed to the design and implementation of the research equally.

References

1. Varshney AK, Mainuddin SG, Nayak J. High power lasers for directed energy applications: Developments and challenges. Infrared Phys Technol. 2024;136:105064. https://doi.org/10.1016/j.infrared.2023.105064.
2. Xu C, Varaprasad BSDCS, Laughlin DE, Zhu J-G. Bias sputtering of granular L10-FePt films with hexagonal boron nitride grain boundaries. Sci Rep. 2023;13(1):11087. https://doi.org/10.1038/s41598-023-38106-9.
3. Xu C, Zhou B, Du T, Varaprasad BSDCS, Laughlin DE, Zhu J-G. Understanding the growth of high-aspect-ratio grains in granular L1-FePt thin-film magnetic media. APL Mater. 2022;10(5). https://doi.org/10.1063/5.0089009.
4. Abdulmalek NM, Dhahir MK. Laser densification of prepared SiO2 Sol-Gel thin films. Baghdad Sci.J. 2018;15(2):0234.

https://bsj.uobaghdad.edu.iq/index.php/BSJ/article/view/2467.
5. Masai H, Kimura H, Kitamura N, Ikemoto Y, Kohara S, Masuno A, *et al.* Densification in transparent SiO2 glasses prepared by spark plasma sintering. Sci Rep. 2022;12(1):14761. https://doi.org/10.1038/s41598-022-18892-4.
6. Eissa D, Hegab RH, Abou-Shady A, Kotp YH. Green synthesis of ZnO, MgO and SiO2 nanoparticles and its effect on irrigation water, soil properties, and Origanum majorana productivity. Sci Rep. 2022;12(1):5780. https://doi.org/10.1038/s41598-022-09423-2.
7. Kono Y, Ohara K, Kondo N M, Yamada H, Hiroi S, Noritake F, *et al.* Experimental evidence of tetrahedral symmetry breaking in SiO2 glass under pressure. Nat Commun. 2022;13(1):2292. https://doi.org/10.1038/s41467-022-30028-w.
8. Idris MS, Subramani S. Nanostructures multilayer MgO/ZnO thin film thermal interface material for LED applications: Thermal, optical, and surface temperature performance. J Mater Sci Mater Electron. 2021;32(12):16008-23. https://doi.org/10.1007/s10854-021-06151-7.
9. l-Rawi MF, Mohammed AM, AL-Duliami HK. Studying the effect of magnesium oxide nanoparticles prepared on the surface of poly methyl methacrylate. Baghdad Sci. J. 2020;17(2):0642. https://bsj.uobaghdad.edu.iq/index.php/BSJ/article/view/4119.
10. Tozman P, Isogami S, Suzuki I, Bolyachkin A, Sepehri-Amin H, J Greaves S, *et al.* Dual-layer FePt-C granular media for multi-level heat-assisted magnetic recording. Acta Mater. 2024;271:119869. https://doi.org/10.1016/j.actamat.2024.119869.
11. Meo A, Pantasri W, Daeng-am W, Rannala S E, Ruta S I, Chantrell R W, *et al.* Magnetization dynamics of granular heat-assisted magnetic recording media by means of a multiscale model. Phys Rev B. 2020;102(17):174419. https://link.aps.org/doi/10.1103/PhysRevB.102.174419.
12. Abdul-Hussain MA, Mohamad H. J. Thermal effect in a 3-D simulation within multilayer thin film of ultraf ast-pulsed laser. MJS. 2021;32(4):104–9. https://mjs.uomustansiriyah.edu.iq/index.php/MJS/article/view/1039.
13. Tom RM, Smith R, Ruiz O, Dai Q, Bogy DB. Optical forces in heat-assisted magnetic recording head-disk interface. Sci Rep. 2023;13(1):8451. https://doi.org/10.1038/s41598-023-35126-3.
14. Chen Y, Victora RH. Effectiveness of a pulsed laser in heat-assisted magnetic recording. Sci Rep. 2023;13(1):11479. https://doi.org/10.1038/s41598-023-38398-x.
15. Greaves SJ. Ultra-fast dynamics for heat-assisted magnetic recording. In: Andreoni W, Yip S, editors. Handbook of Materials Modeling: Applications: Current and Emerging Materials. Cham: Springer Int Pub; 2020. p. 449–66. https://doi.org/10.1007/978-3-319-44680-6_106.
16. Mirkoohi E, Seivers DE, Garmestani H, Liang SY. Heat source modeling in selective laser melting. Materials (Basel). 2019;12(13):2052. https://doi.org/10.3390/ma12132052.
17. Hotta S. Reflection and transmission of electromagnetic waves in dielectric media. In: Hotta S, Eds. Mathematical Physical Chemistry: Practical and Intuitive Methodology. Singapore: Springer Nat Sing; 2023. p. 305–50. https://doi.org/10.1007/978-981-99-2512-4_8.
18. Macchi A, Moruzzi G, Pegoraro F. Problems in Classical Electromagnetism: 203 Exercises with Solutions. Cham: Springer Int Pub; 2023. p. 99–110. https://doi.org/10.1007/978-3-031-22235-1_11.
19. Chernyshov A, Treves D, Le T, Zong F, Ajan A, Acharya R. Measurement of FePt thermal properties relevant to heat-assisted magnetic recording. J Appl Phys. 2014;115(17). https://doi.org/10.1063/1.4866519.
20. Nfawa SR, Abu Talib AR, Basri AA, Masuri SU. Novel use of MgO nanoparticle additive for enhancing the thermal conductivity of CuO/water nanofluid. Case Stud Therm Eng. 2021;27:101279. https://www.sciencedirect.com/science/article/pii/S2214157X21004421.
21. Andrew S, Bernard F, Phelps J. Thermal conductivity of magnesium oxide from absolute, steady-state measurements. J Res Natl Inst Stand Technol. 1998;103(4). http://dx.doi.org/10.6028/jres.103.021.
22. Zhu W, Zheng G, Cao S, He H. Thermal conductivity of amorphous SiO2 thin film: A molecular dynamics study. Sci Rep. 2018;8(1):10537. https://doi.org/10.1038/s41598-018-28925-6.
23. Gevariya BH, Patel SJ, Kheraj V, editors. Determination of Thickness and Refractive Indices of Thin Films from Reflectivity Spectrum Using Rao-1 Optimization Algorithm. AIP Conf Proc; 2023; Singapore. https://doi.org/10.1007/978-981-99-2854-5_7.
24. Wang X, Zeng S, Wang Z, Ni J. Identification of crystalline materials with ultra-low thermal conductivity based on machine learning study. J Phys Chem C. 2020;124(16):8488–95. https://doi.org/10.1021/acs.jpcc.9b11610.
25. Zhan T, Xu M, Cao Z, Zheng C, Kurita H, Narita F, *et al.* Effects of thermal boundary resistance on thermal management of gallium-nitride-based semiconductor devices: A review. Micromachines. 2023;14(11):2076. https://doi.org/10.3390/mi14112076.
26. Heijmans K, Pathak AD, Solano-López P, Giordano D, Nedea S, Smeulders D. Thermal boundary characteristics of homo-/heterogeneous interfaces. Nanometers. 2019;9(5):663. https://doi.org/10.3390/nano9050663.

محاكاة حرارية لليزر فائق السرعة في عينة متعددة الطبقات لتطبيق التسجيل المغناطيسي بمساعدة الحرارة

حيدر جواد محمد ، بسعاد هادي حمزة

قسم الفيزياء، كلية العلوم، الجامعة المستنصرية، بغداد، العراق.

الخلاصة

تعتبر تقنية التسجيل المغناطيسي بمساعدة الحرارة (HAMR) خطوة واعدة في توسيع سعة القرص الصلب .تعتمد هذه التقنية على الليزر فائق السرعة لإزالة المغناطيسية من الطبقة وتسجيل البيانات على القرص الصلب أو أي وسائط تخزين. ومع ذلك، فإن وصفة الطبقات صعبة وتمنح مساحة للاستكشاف. كان التحقيق في تأثيرات ملف تعريف درجة الحرارة والتدرج الحراري على العينة المقترحة(FePt (8nm) / MgO (8nm) /SiO2 (58nm) / Si (9.32E-7nm لاستخدام HAMR هو محور هذه الدراسة. يعطي محاكاة الطبقات المتعددة رؤية لسلوك الليزر فائق السرعة) كثافة الطاقة $1.7923\ E14\ W/m^2$ بطول موجي 800 نانومتر (داخل مجموعة العينات يتم حساب الاعتبار البصري اعتمادًا على الضوء الساقط والمنعكس والمنتقل على السطح بين الطبقات. يلعب سمك طبقة العينة دورًا حاسمًا في تقليل طاقة الليزر. يساعد التدرج في درجة الحرارة داخل العينة في اختيار طاقة الليزر المناسبة، والتي يتم استخدامها مع تقنية HAMR . تظهر النتائج تأثير درجة الحرارة على سمك العينة ودرجة الحرارة كقوة ليزر. بعد ذلك من الواضح أي سمك وقوة ليزر يمكن استخدامها بكفاءة.

الكلمات المفتاحية: المحاكاة البصرية، تقنية HAMR، الليزر فائق السرعة، جهاز سبترونك، تخزين البيانات.